Supplementary Information for "Li-ion intercalation-driven control of two-dimensional magnetism in van der Waals $FePS_3$ bilayers†"

Dong Chen [*a], Chunlei Wang [a] and Chengxiao Peng [b]

[a] *College of Physics and Electronic Engineering, Xinyang Normal University, Xinyang 464000, P. R. China*

[b] *Institute for Computational Materials Science, International Joint Research Laboratory of New Energy Materials and Devices of Henan Province, School of Physics and Electronics, Henan University, Kaifeng 475004, P. R. China*

1. Three-dimensional (3D) $FePS_3$ bulks

Table S1 Optimized crystal structure (lattice parameters *a, b, c, β*, total energy difference Δ*E* per Fe ion, and average magnetic moment *m*) of the 3D bulk $FePS_3$ with nonmagnetic (NM), ferromagnetic (FM), and antiferromagnetic (AFM) orders

$FePS_3$	*a* /Å	*b* /Å	*c* /Å	*β* /°	*m* /μ_B	Δ*E* per Fe ion /meV
NM	5.713	9.723	6.283	105.4	0.00	1116.07
FM (↑↑↑↑)	5.916	10.116	6.648	105.2	3.60	359.95
AFM1(↓↓↑↑)	5.928	10.185	6.669	105.5	3.57	17.76
AFM2(↓↑↓↑)	5.925	10.183	6.617	105.6	3.56	0.00
AFM3(↓↑↑↓)	5.923	10.178	6.680	105.5	3.57	0.72
AFM4(↑↓↓↑)	5.923	10.178	6.686	105.5	3.57	0.70
AFM5(↑↓↑↓)	5.924	10.188	6.607	105.6	3.55	0.21
AFM6(↑↑↓↓)	5.928	10.185	6.669	105.5	3.57	17.75
Expt. [1]	5.940[1]	10.260[1]	9.898[1]	108.3[1]	4.52[1]	AFM order [1]
Expt. [2]	5.943[2]	10.299[2]	6.716[2]	107.3[2]	3.56[3]	AFM order [2]
Expt. [4]	5.947[4]	10.300[4]	6.722[4]	107.1[4]	3.68[5]	AFM order [4]
Calc. [6]	5.861[6]	10.047[6]	6.600[6]	108.1[6]	3.70-4.0[7]	AFM order [6]

Three-dimensional (3D) $FePS_3$ crystal has a monoclinic structure with the space group of

C2/m, as shown in Fig. S1. Two kinds of non-equilibrium FeI and FeII atoms are located at the [FeI: Fe1 (0, 0.3330, 0) and Fe2 (0, 0.6669, 0)] and [FeII: Fe3 (0.5000, 0.8330, 0) and Fe4 (0.5000, 0.1669, 0)] Wyckoff positions, respectively. The total energy difference ΔE can be defined as $\Delta E = E - E_L$, where E and E_L are the total energies for a fixed magnetic structure [nonmagnetic (NM), ferromagnetic (FM), or antiferromagnetic (AFM)] and the lowest-energy structure (AFM2 order), respectively. The most stable structure, which is obtained by the minimum energy criterion [8] of the 3D bulk $FePS_3$, corresponds to the AFM2(↓↑↓↑) structure. The ↓, ↑, ↓, and ↑ arrows represent the spin directions of Fe1(spin-down), Fe2(spin-up), Fe3(spin-down), and Fe4(spin-up) atoms, respectively. The highest energy is associated with the NM structure, primarily due to the magnetic nature of Fe. This suggests that the NM order of the $FePS_3$ bulk is unstable. Our calculated lattice parameters *a, b, c, β*, and average magnetic moment *m* are in good agreement with previous data [1-7]. The ground-state structure (AFM2 order) of the bulk $FePS_3$ is illustrated in Fig. S1, illustrating the Wyckoff positions and magnetic spins of different atoms. Tests of Hubbard-*U* and different generalized gradient approximation/local density approximation (GGA/LDA) functionals are shown in Tables. S2 and S3, respectively.

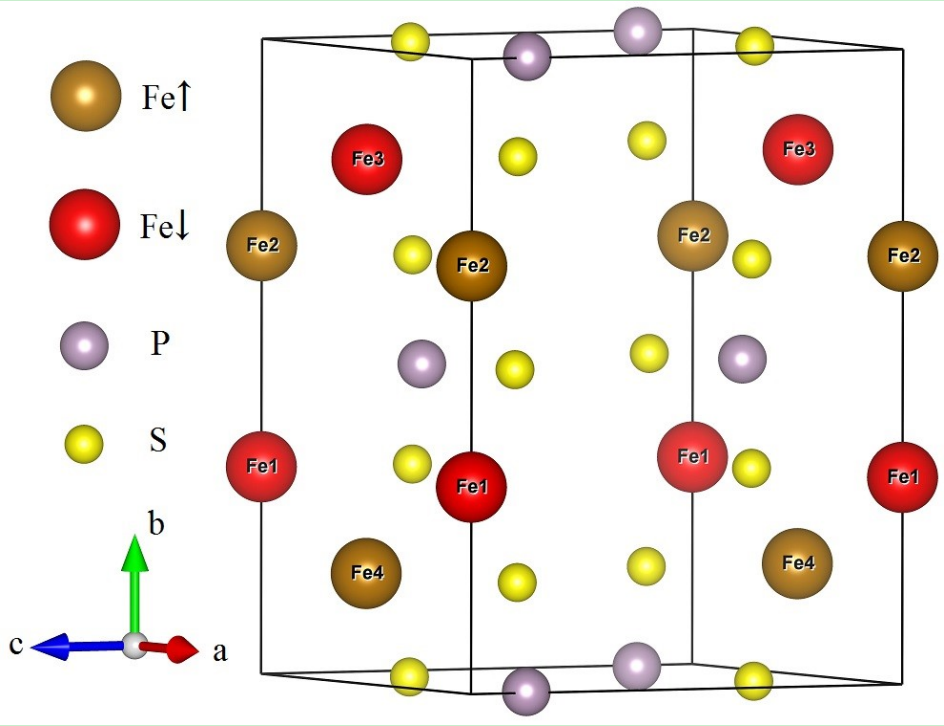

Fig. S1 Ground-state crystal structure of bulk $FePS_3$. Large khaki spheres, large red spheres, purple, and yellow spheres represent the Fe (spin-up), Fe (spin-down), P, and S atoms, respectively.

Table S2 Calculated ground-state lattice parameters *a, b, c*, and average magnetic moment *m* of Fe ions of the bulk $FePS_3$ material with the Perdew-Burke-Ernzerhof (PBE) functional

Hubbard-*U*	*a* /Å	*b* /Å	*c* /Å	*m* /μ_B
U = 1 eV	5.918	10.177	6.569	3.40
U = 2 eV	5.854	10.276	6.572	3.43
U = 3 eV	5.925	10.183	6.617	3.56
U = 4 eV	5.884	10.303	6.622	3.59
U = 5 eV	5.899	10.318	6.643	3.67
U = 6 eV	5.913	10.332	6.657	3.73
U = 7 eV	5.924	10.343	6.668	3.78

Table S3 Calculated lattice parameters *a*, *b*, *c*, and average magnetic moment *m* of Fe ions with different functionals

Functionals (with Hubbard-*U* = 3 eV)	*a* /Å	*b* /Å	*c* /Å	*m* /μ_B
Perdew-Burke-Ernzerhof (PBE)	5.925	10.183	6.617	3.56
Perdew-Burke-Ernzerhof revised for solids (PBEsol)	5.882	10.136	6.438	3.51
revised Perdew-Burke-Ernzerhof (rPBE)	5.898	10.138	6.497	3.53
Perdew-Wang 91 (PW91)	5.760	10.071	6.333	1.94
Local Density Approximation (LDA)	5.727	10.064	6.282	3.36
Armiento-Mattson 05 (AM05)	5.890	10.155	6.566	3.50

The relationship between the Hubbard-*U* (GGA/LDA functionals) and the ground-state structural properties of bulk $FePS_3$ is presented in Table S2 (Table S3). As can be seen in Tables S1 and S2, our calculation parameters, especially the Hubbard-*U* value (*U* = 3 eV), yield accurate lattice parameters *a, b, c*, and average magnetic moment *m* of 3D $FePS_3$ [1-7]. The PBE functional is found to be suitable for the calculation because it shows more accurate results compared to other functionals, as shown in Table S3. The same or similar values of *U* (*U* = 3 eV [9], 3 eV [3], 3 eV [10], and 3.5 eV [11]) are used in previous studies to treat the on-site Coulomb interactions of 3D $FePS_3$. This suggests the significance of the chosen U value in accurately describing the fundamental properties of $FePS_3$. Besides, the density functional theory (DFT) calculations with GGA-PBE functional have been widely employed in electronic structure calculations for both 3D $FePS_3$ bulks [12, 13] and 2D $FePS_3$ monolayers/multilayers [3, 12, 14, 15].

More importantly, our calculated band gap of bulk $FePS_3$ is 1.55 eV, which is in good agreement with previous experimental data {(1.60 eV) [16], (1.50 eV) [17]} and theoretical results {(1.80 eV) [6], (1.54 eV) [18]}. For the bulk $FePS_3$ material, we conclude that the PBE functional and the Hubbard-U (U = 3 eV) can get accurate and reliable results. Consequently, the parameters (PBE functional and Hubbard-U = 3 eV) are considered in the calculation of two-dimensional (2D) $FePS_3$ thin layers due to the reason that there are almost no Hubbard-U values can be found for the 2D $FePS_3$ (FPS) system. Since it is challenging to find specific parameters for 2D FPS, it is reasonable to utilize those above-mentioned parameters that have been successful in describing the 3D bulk FPS material.

2. Two-dimensional (2D) $FePS_3$ bilayers

In this section, we present the models and calculation methodology of the 2D $FePS_3$ bilayers. It is noteworthy that the monolayer/few-layer $FePS_3$ has already been experimentally synthesized [19-21]. More importantly, Du et al. [22] first realized the mechanically fabricated 2D MPS_3 (M = Fe, Mn, Ni, Cd, and Zn) sulfide family, and finally, they ultimately obtained the 2D $FePS_3$ monolayer. We highlight two important aspects: (1) The 2D $FePS_3$ thin films are mechanically stable even down to the monolayer regime, as shown in Refs. [9, 20]; (2) Some ions such as Mg [23] and polyethylene oxide PEO [24] ions with larger radii than the Li ion and the Li ion itself [25] have already been intercalated into the FPS thin layers, and their crystal structures remain stable. Therefore, it is not necessary to calculate and plot the phonon spectrum of our bilayers to show the mechanical stabilities of our 2D FPS, 1Li- and 2Li-intercalated FPS bilayers since they are inherently stable.

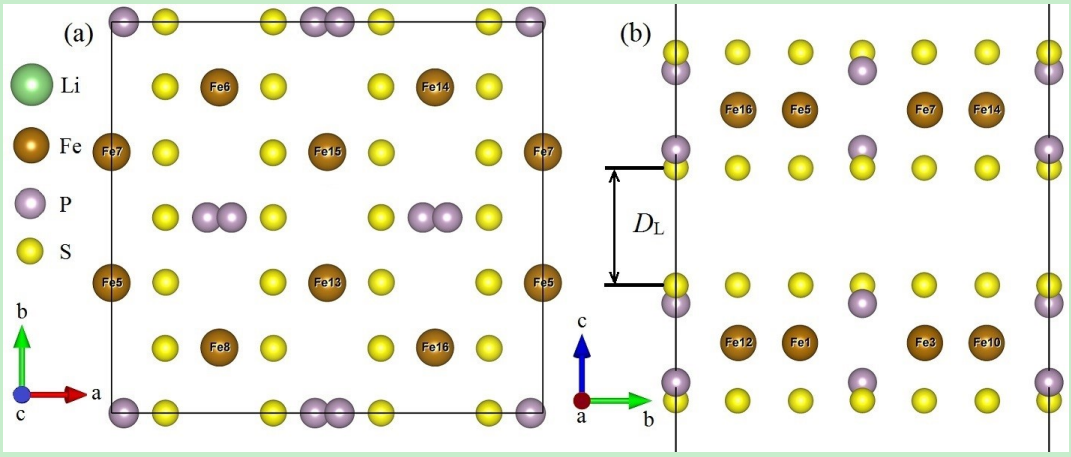

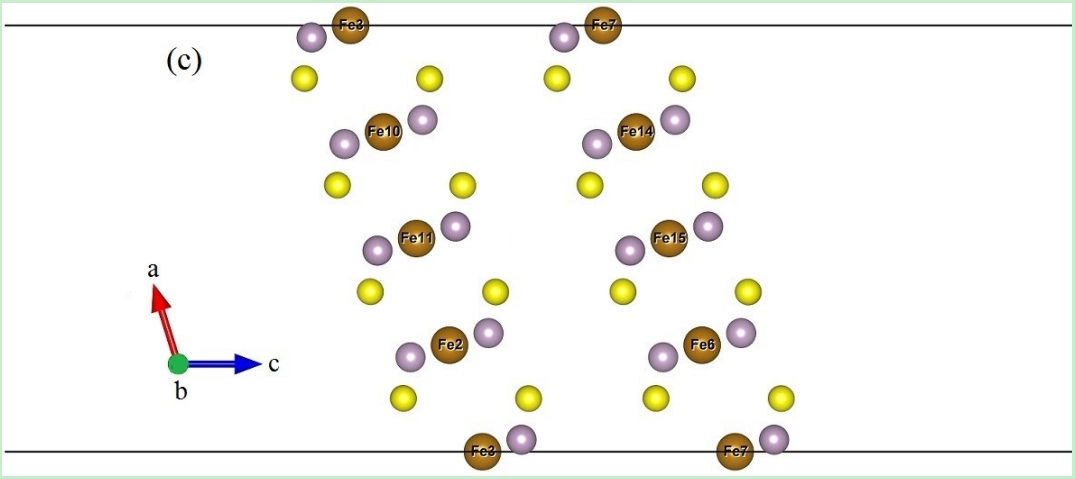

Fig. S2 Top view (a) and side views along the *a*-axis (b) and *b*-axis (c) of the 2D $FePS_3$ bilayer.

The top view and side views of the 2D $FePS_3$ bilayers are drawn in Fig. S2. Our 2D bilayer contains two $FePS_3$ monolayers, each monolayer contains two S sublayers, two P sublayers, and one Fe sublayer [26]. We built a 2×1 supercell along the *a*- and *b*-axes, respectively. A vacuum space of 20 Å is built to minimize the interlayer interactions between the adjacent bilayers. Finally, our 2D system contains 16 Fe, 16 P, and 48 S atoms, which can better describe the AFM and ferrimagnetic (FiM) orders than the conventional $FePS_3$ unit cell (which contains only 4 Fe atoms). The fractional coordinates of Fe in the 2D FPS, 1Li-FPS, and 2Li-FPS bilayers are Fe1 (0, 0.3326, 0.4000), Fe2 (0.2500, 0.8326, 0.4000), Fe3 (0, 0.6674, 0.4000), Fe4 (0.2500, 0.1674, 0.4000), Fe5 (0, 0.3326, 0.6000), Fe6 (0.2500, 0.8326, 0.6000), Fe7 (0, 0.6674, 0.6000), Fe8 (0.2500, 0.1674, 0.6000), Fe9 (0.5000, 0.3326, 0.4000), Fe10 (0.7500, 0.8326, 0.4000), Fe11 (0.5000, 0.6674, 0.4000), Fe12 (0.7500, 0.1674, 0.4000), Fe13 (0.5000, 0.3326, 0.6000), Fe14 (0.7500, 0.8326, 0.6000), Fe15 (0.5000, 0.6674, 0.6000), and Fe16 (0.7500, 0.1674, 0.6000).

Table S4 Total energy difference Δ*E* per Fe atom (meV) of the NM, FM, AFM, and ferrimagnetic (FiM) orders of the 2D $FePS_3$ bilayer

Magnetic orders	Spin states	Δ*E* per Fe /meV
NM	No spin	1135.19
FM	↑↑↑↑↑↑↑↑↑↑↑↑↑↑↑↑	106.96
AFM1	↑↑↑↑↓↓↓↓↑↑↑↑↓↓↓↓	104.84
AFM2	↑↓↑↓↑↑↑↑↓↑↓↑↓↓↓↓	8.04
AFM3	↓↑↓↑↓↓↓↓↑↓↑↓↑↑↑↑	7.75

AFM4	↓↓↓↓↓↓↓↑↑↑↑↑↑↑↑	7.21
AFM5	↓↓↓↓↓↑↓↑↑↑↑↑↑↓↑↓	7.75
AFM6	↓↑↓↑↓↑↓↑↓↑↓↑↓↑↓↑	90.72
AFM7	↓↓↑↑↑↑↓↓↓↑↓↑↓↑↓↑	7.71
AFM8	↓↓↑↑↓↓↑↑↓↑↓↑↓↑↓↑	7.56
FiM1	↓↓↑↑↓↑↑↑↑↑↑↑↑↑↑↑	8.85
FiM2	↓↑↓↑↑↑↓↑↑↑↑↑↑↑↑↑	8.45
FiM3	↑↓↑↑↓↑↑↑↓↑↑↑↑↑↑↑	6.28
FiM4	↑↑↑↓↑↑↑↑↓↑↑↑↑↓↑↑	4.74
FiM5	↑↑↓↑↑↑↑↓↑↑↑↑↑↑↓	9.03
FiM6	↑↓↑↑↑↑↑↑↓↓↑↑↑↑↑	4.99
FiM7	↑↑↑↑↓↑↑↑↑↓↑↑↓↑↑	6.22
FiM8	↑↑↑↓↑↑↑↑↑↑↓↑↑↑↓	6.71
FiM9	↑↓↑↑↑↓↑↑↑↑↓↑↑↑↓	11.76
FiM10	↓↑↑↑↓↑↑↑↑↓↑↑↑↓↑	11.72
FiM11	↑↓↑↑↑↓↑↑↑↓↑↑↑↓↑↑	11.17
FiM12	↑↑↑↓↑↑↑↓↑↑↑↓↑↑↑↓	5.74
FiM13	↓↑↑↑↓↑↑↑↓↑↑↑↓↑↑↑	10.62
FiM14	↑↑↓↑↑↑↓↑↑↑↓↑↑↑↓↑	10.62
FiM15	↑↓↑↑↑↓↑↑↓↑↑↑↓↑↑↑	5.62
FiM16	↑↑↑↓↑↑↑↓↑↑↓↑↑↑↓↑	5.62
FiM17	↑↓↑↑↑↓↑↓↑↑↑↑↓↑	4.67
FiM18	↑↑↑↓↑↑↓↑↓↑↑↑↑↓↑	7.01
FiM19	↑↑↓↑↓↑↑↑↓↑↑↑↑↓↑	11.98
FiM20	↑↓↓↓↓↑↑↑↑↑↑↑↑↑↑	6.62
FiM21	↑↑↓↑↑↑↓↑↓↑↓↑↑↑↓↑	7.90
FiM22	↑↑↑↓↑↑↑↓↑↑↑↓↑↓↑↓	8.61
FiM23	↓↑↓↑↑↑↑↓↑↑↓↑↑↓↑	5.13
FiM24	↑↓↓↑↑↑↑↓↑↑↑↑↓↑↓	6.95
FiM25	↑↑↓↑↓↑↓↑↓↑↑↑↓↑↓↑	14.01
FiM26	↑↓↑↑↑↑↓↑↓↑↑↓↑↓↓	5.47
FiM27	↓↓↓↓↓↑↑↑↑↑↑↑↑↑↑	5.93
FiM28	↑↓↑↑↓↑↑↑↓↑↓↑↓↑↑↓	0.00
FiM29	↑↑↓↑↑↑↑↓↑↑↑↑↑↑↑	10.80
FiM30	↑↑↑↑↑↓↑↑↑↑↑↑↑↑↑	14.88

In this work, one NM, one FM, eight AFM, and thirty ferrimagnetic (FiM) structures are considered for 2D $FePS_3$, as listed in Table S4. The total energy difference per Fe atom (ΔE) can be described as $\Delta E = E_f - E_{FiM28}$, where E_f and E_{FiM28} are the total energies for a fixed magnetic structure (NM, FM, AFM, and FiM) and the lowest-energy 2D structure (FiM28: ↑↓↑↑↓↑↑↑↓↑↓↑↓↑↑↓), respectively. Since the Fe ion itself has a magnetic nature, the ΔE of the NM structure is very high. Such high energy confirms that the NM structure is not energetically favorable. Besides, the optimized interlayer spacing D_L between the two monolayers [shown in Fig. S2(b)] is 3.30 Å, reflecting a van der Waals (vdW) nature of our 2D bilayer since vdW materials usually have interlayer spacings of 3～4 Å. Our vdW gap is in excellent agreement with previous data of 2D $FePS_3$ thin films (3.38 Å [6] and 3.26 Å [27]).

Now, we discuss the Li-ion intercalation scheme. According to the 2D symmetry of our $FePS_3$ bilayer and the sizes of interstitial sites, we have considered six possible positions that can be occupied by the Li ion. The most probable position of Li-ion is determined by the minimum total energy criteria [8], where the structure with the lowest total energy is considered the most favorable.

Table S5 Ground-state lattice parameters *a, b* (Å) and total energy difference per Fe ion (meV) of the 1Li-intercalated $FePS_3$ bilayers (1Li-FPS) with different Wyckoff positions of Li

Structures	Coordinates of the Li-ion	ΔE /meV	*a* /Å	*b* /Å
Structure 1Li-1	0.5000, 0.5000, 0.5000	0.00	11.82	10.239
Structure 1Li -2	0.5288, 0.5260, 0.3791	24.57	11.82	10.249
Structure 1Li -3	0.7161, 0.6680, 0.4018	5.34	11.83	10.240
Structure 1Li -4	0.1270, 0.1928, 0.3996	24.11	11.83	10.243
Structure 1Li -5	0.1307, 0.8439, 0.3959	22.67	11.82	10.247
Structure 1Li -6	0.5000, 0.5000, 0.3990	94.72	11.90	10.265

In Table S5, the calculated total energy difference ΔE is defined as $\Delta E = E_1 - E_b$, where E_1 and E_b are the total energies of Structure 1Li-1 and Structures 1Li-b (b = 2, 3, 4, 5, 6), respectively. Take Structure 1Li-1 as an example, where "1Li" denotes the presence of one Li ion in the 2D FPS system, while "1" corresponds to the first structure with the Li ion occupying the Wyckoff position (0.5000, 0.5000, 0.5000). The most stable structure of the 1Li-intercalated $FePS_3$ bilayer (1Li-FPS), which has the lowest total energy, corresponds to Structure 1Li-1 (refer to Fig. S3).

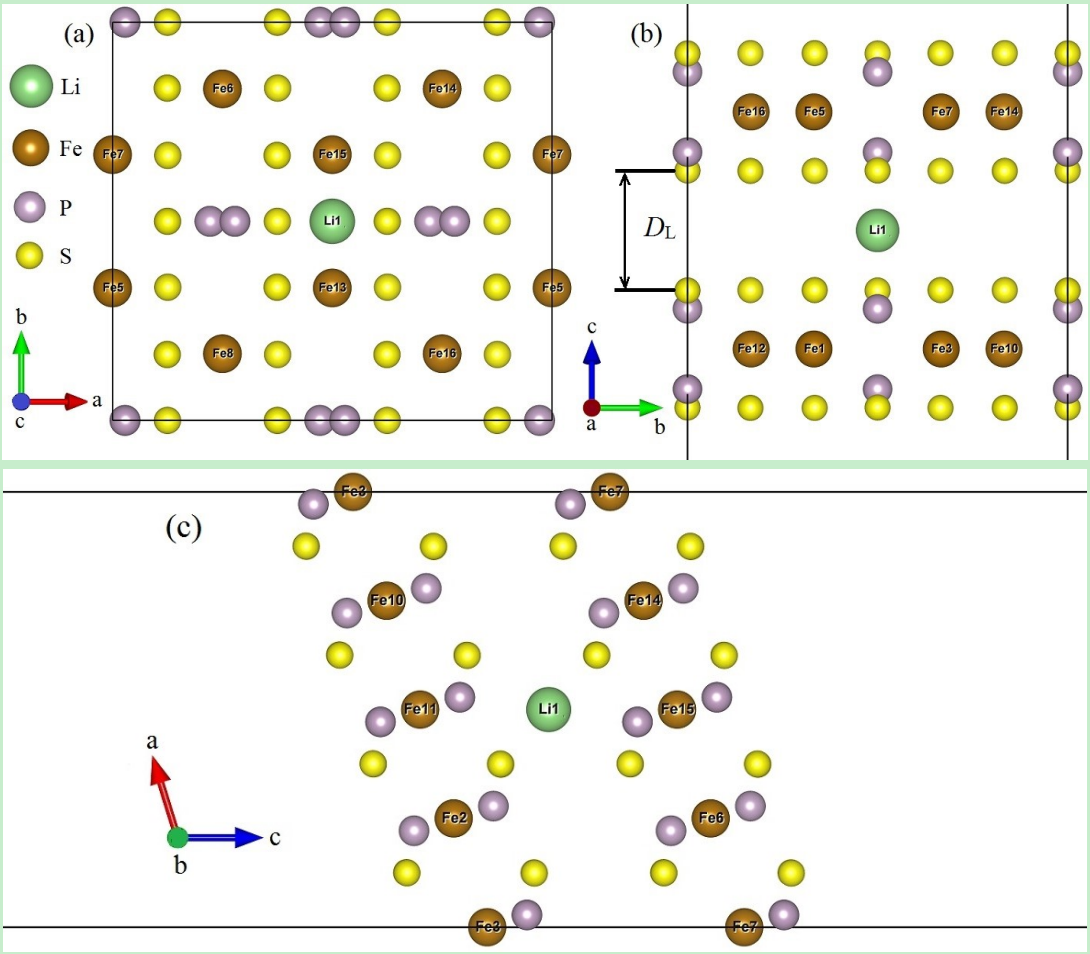

Fig. S3 Top view (a) and side views of the 1Li-intercalated $FePS_3$ bilayer along the *a*-axis (b) and *b*-axis (c) with the most stable position of the Li ion before geometry optimization.

Table S6 Ground-state lattice parameters *a, b* (Å) and total energy difference Δ*E* per Fe ion (meV) of the 2Li-intercalated $FePS_3$ bilayers with different positions of Li

Structures	Coordinates of the two Li-ions	Δ*E* /meV	*a* /Å	*b* /Å
Structure 2Li-1	Li1 (0.7434, 0.7426, 0.4957) Li2 (0.2499, 0.2501, 0.5029)	8.13	11.837	10.254
Structure 2Li-2	Li1 (0.5000, 0.2500, 0.5000) Li2 (0.5000, 0.7500, 0.5000)	3.96	11.841	10.266
Structure 2Li-3	Li1 (0.6074, 0.7621, 0.5962) Li2 (0.3546, 0.2635, 0.6059)	14.85	11.859	10.252
Structure 2Li-4	Li1 (0.5945, 0.9147, 0.3997) Li2 (0.3729, 0.2635, 0.5991)	42.10	11.849	10.260
Structure 2Li-5	Li1 (0.2500, 0.5000, 0.5000) Li2 (0.7500, 0.5000, 0.5000)	0.00	11.829	10.259
Structure 2Li-6	Li1 (0.6286, 0.5031, 0.4037) Li2 (0.3801, 0.4968, 0.6002)	62.20	11.841	10.265

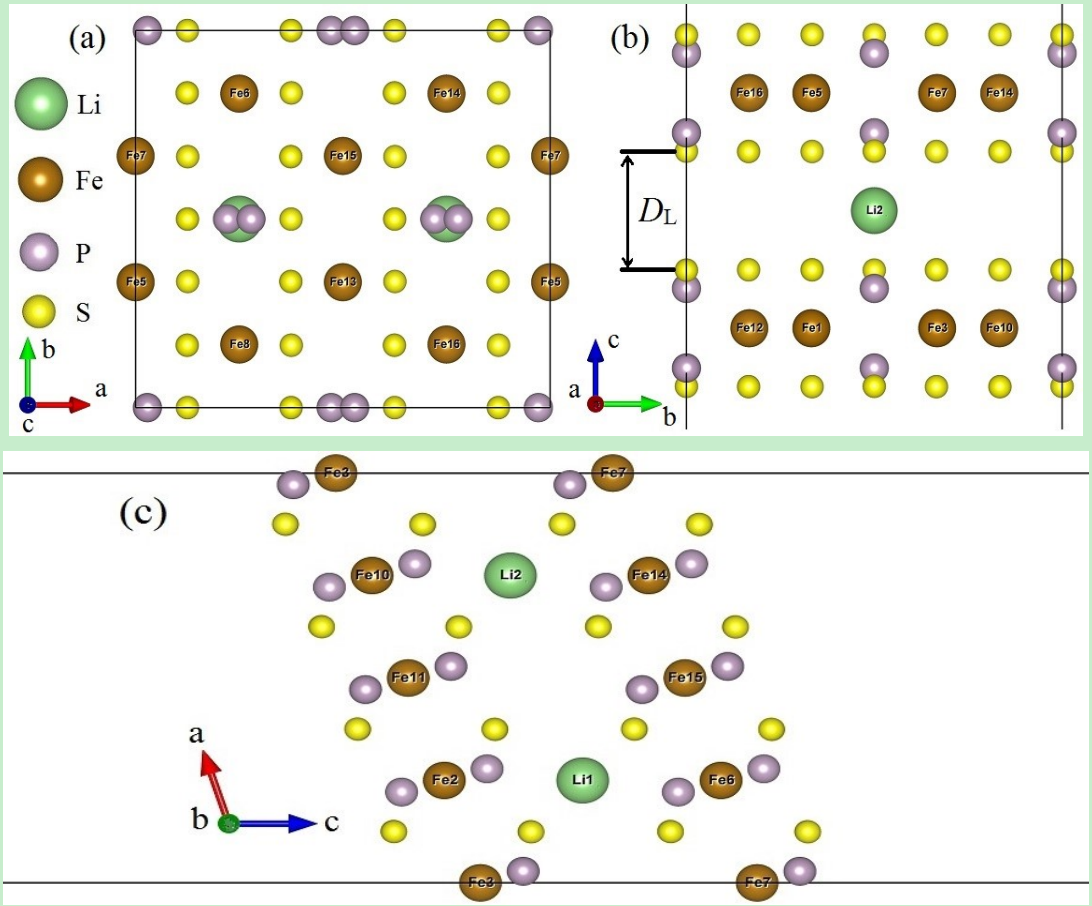

Fig. S4 Top view (a) and side views of the 2Li-intercalated $FePS_3$ bilayer along the *a*-axis (b) and *b*-axis (c) with the most stable Wyckoff positions of two Li ions before geometry optimization.

Table S7 Total energy difference ΔE per Fe atom (meV) for the NM, FM, AFM, and FiM structures of the 1Li- (1Li-FPS) and 2Li-intercalated $FePS_3$ bilayers (2Li-FPS)

Magnetic orders	Spin states	ΔE /meV (1Li-FPS)	ΔE /meV (2Li-FPS)
NM	No spin	1175.32	1201.96
FM	↑↑↑↑↑↑↑↑↑↑↑↑↑↑	10.72	0.00
AFM1	↑↑↑↑↓↓↓↓↑↑↑↑↓↓↓↓	9.11	7.09
AFM2	↑↓↑↓↑↑↑↑↓↑↓↑↓↓↓↓	0.31	3.10
AFM3	↓↑↓↑↓↓↓↓↑↓↑↓↑↑↑↑	0.33	6.96
AFM4	↓↓↓↓↓↓↓↓↑↑↑↑↑↑↑↑	0.00	2.98
AFM5	↓↓↓↓↓↑↓↑↑↑↑↑↑↓↑↓	1.28	4.38
AFM6	↓↑↓↑↓↑↓↑↓↑↓↑↓↑↓↑	23.39	26.49
AFM7	↓↓↑↑↑↑↓↓↓↑↓↑↓↑↓↑	8.10	14.45
AFM8	↓↓↑↑↓↓↑↑↓↑↓↑↓↑↓↑	9.53	14.28
FiM1	↓↓↑↑↓↑↑↑↑↑↑↑↑↑↑	2.77	6.84
FiM2	↓↑↓↑↑↑↓↑↑↑↑↑↑↑↑	3.17	7.13
FiM3	↑↓↑↑↓↑↑↑↓↑↑↑↑↑↑	4.22	8.71

FiM4	↑↑↑↓↑↑↑↑↓↑↑↑↑↓↑↑	2.43	5.26
FiM5	↑↑↓↑↑↑↑↑↓↑↑↑↑↑↑↓	5.38	75.95
FiM6	↑↓↑↑↑↑↑↑↓↓↑↑↑↑↑	6.02	7.64
FiM7	↑↑↑↑↓↑↑↑↑↓↑↑↓↑↑	6.14	8.24
FiM8	↑↑↑↓↑↑↑↑↑↑↓↑↑↑↓	6.68	8.25
FiM9	↑↓↑↑↑↓↑↑↑↑↑↓↑↑↑↓	16.74	15.63
FiM10	↓↑↑↑↓↑↑↑↑↓↑↑↑↓↑	9.88	15.27
FiM11	↑↓↑↑↑↓↑↑↑↓↑↑↑↓↑↑	7.92	4.81
FiM12	↑↑↑↓↑↑↑↓↑↑↑↓↑↑↑↓	6.58	7.04
FiM13	↓↑↑↑↓↑↑↑↓↑↑↑↓↑↑↑	3.17	12.69
FiM14	↑↑↓↑↑↑↓↑↑↑↓↑↑↑↓↑	3.18	3.93
FiM15	↑↓↑↑↑↓↑↑↓↑↑↑↓↑↑↑	3.39	6.66
FiM16	↑↑↑↓↑↑↑↓↑↑↓↑↑↑↓↑	4.59	10.18
FiM17	↑↓↑↑↑↑↓↑↓↑↑↑↑↓↑	4.01	8.00
FiM18	↑↑↑↓↑↑↓↑↓↑↑↑↑↓↑	6.95	8.77
FiM19	↑↑↓↑↓↑↑↑↓↑↑↑↑↓↑	10.07	27.10
FiM20	↑↓↓↓↓↓↑↑↑↑↑↑↑↑↑	98.39	4.53
FiM21	↑↑↓↑↑↑↓↑↓↑↓↑↑↑↓↑	5.98	10.59
FiM22	↑↑↑↓↑↑↑↓↑↑↑↓↑↓↑↓	9.28	15.37
FiM23	↓↑↓↑↑↑↑↓↑↑↓↑↑↓↑	4.61	7.51
FiM24	↑↓↓↑↑↑↑↓↑↑↑↓↑↓	7.36	12.23
FiM25	↑↑↓↑↓↑↓↑↓↑↑↑↓↑↓↑	14.16	23.24
FiM26	↑↓↑↑↑↑↓↑↓↑↑↓↑↓↓	2.94	3.58
FiM27	↓↓↓↓↓↓↑↑↑↑↑↑↑↑↑	2.69	4.30
FiM28	↑↓↑↑↓↑↑↑↓↑↓↑↓↑↑↓	2.62	7.22
FiM29	↑↑↓↑↑↑↑↓↑↑↑↑↑↑↑	7.08	10.94
FiM30	↑↑↑↑↑↓↑↑↑↑↑↑↑↑↑	8.25	8.53

The ground-state structures of the 1Li-intercalated $FePS_3$ bilayer (1Li-FPS) and 2Li-intercalated $FePS_3$ bilayer (2Li-FPS) are the AFM4 (↓↓↓↓↓↓↓↓↑↑↑↑↑↑↑↑) and FM (↑↑↑↑↑↑↑↑↑↑↑↑↑↑↑↑) structures, respectively. The energy differences (ΔEs) of the two NM structures are found to be quite high due to the magnetic nature of Fe, which reflects that the NM structures may not be stable in 1Li- and 2Li-FPS. Besides, the optimized interlayer spacing D_L between the two monolayers [shown in Figs. S3(b) and S4(b)] are 3.27 and 3.12 Å for the 1Li-FPS and 2Li-FPS bilayers, respectively. This reflects the vdW nature of our 1Li- and 2Li-FPS bilayers since vdW materials typically exhibit interlayer spacings in the range of 3～4 Å. Unfortunately, the authors have not found any available experimental data or theoretical results of the interlayer spacing D_L for the Li-intercalated FPS bilayers.

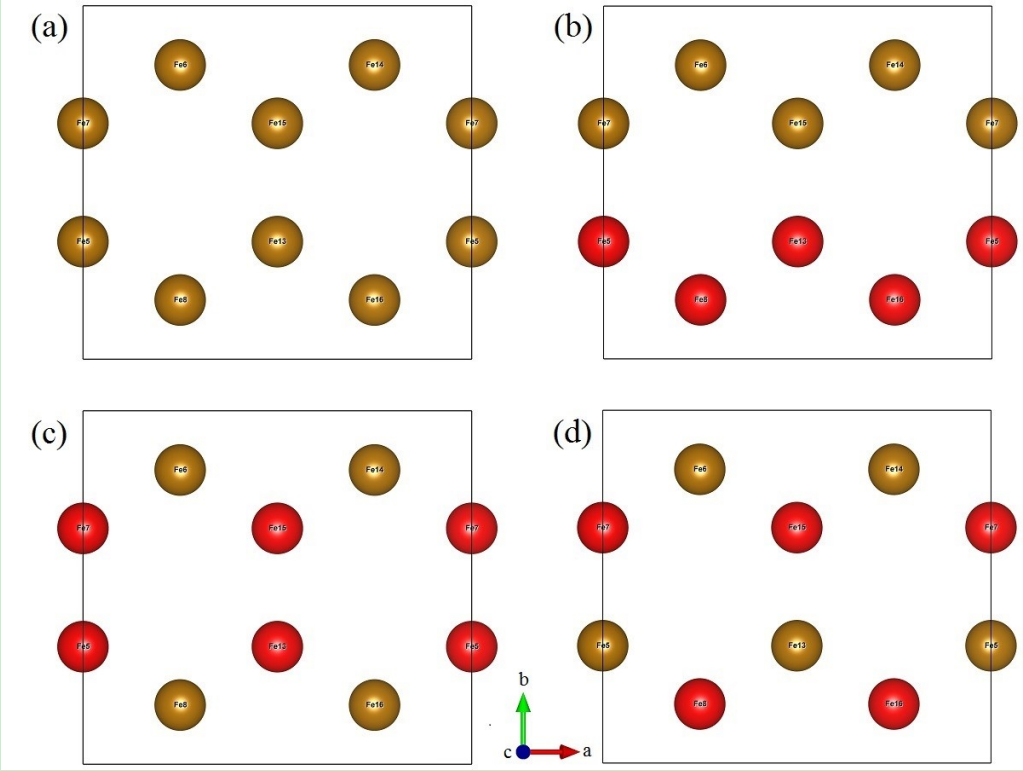

Fig. S5 The schematic structures of different magnetic orders of the FPS, 1Li-FPS, and 2Li-FPS bilayers for the calculation of intraplane exchange couplings J_1, J_2, and J_3: (a) FM configuration [FM]; (b) Zigzag AFM configuration [Z-AFM]; (c) Stripy AFM configuration [S-AFM]; and (d) Néel AFM configuration [N-AFM]. The khaki and red balls represent the Fe (spin-up) and Fe (spin-down) atoms, respectively.

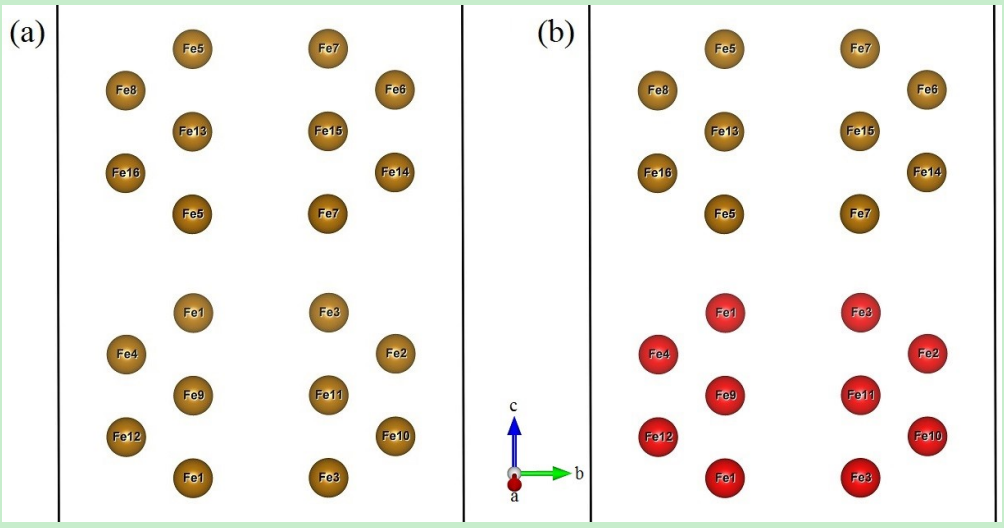

Fig. S6 Schematic structures of different magnetic orders of the FPS, 1Li-FPS, and 2Li-FPS bilayers for the calculation of interplane exchange coupling J_c: (a) FM configuration [FM], and (b) type-A AFM configuration [A-AFM]. The khaki and red balls represent the Fe (spin-up) and Fe

(spin-down) atoms, respectively.

The FM order [FM], Zigzag AFM order [Z-AFM], stripy AFM order [S-AFM], and Néel AFM order [N-AFM] of our FPS, 1Li-FPS, and 2Li-FPS bilayers are shown in Fig. S5. These magnetic configurations are consistent with the magnetic configurations given in Refs. [5, 28]. Besides, the FM order and type-A AFM order [A-AFM] of the three bilayers are presented in Figs. S6(a) and S6(b), respectively.

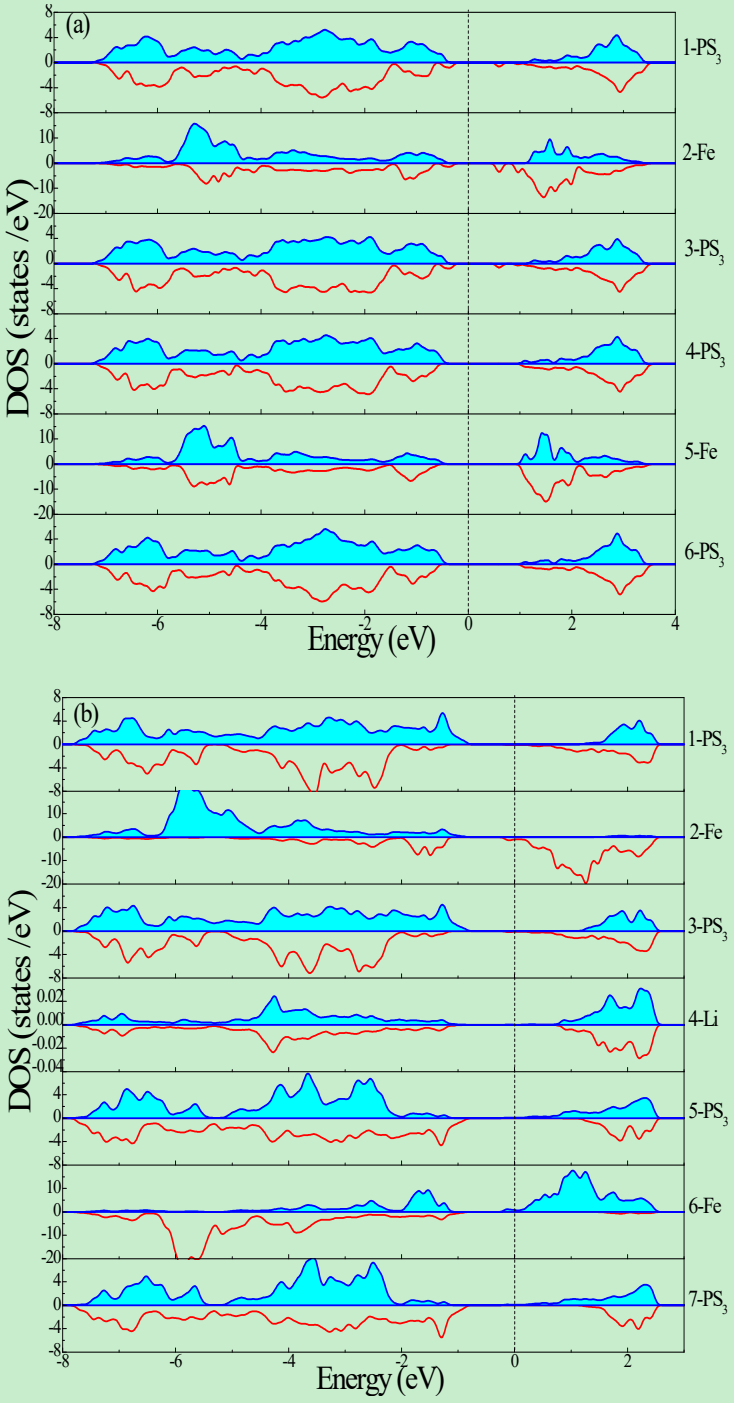

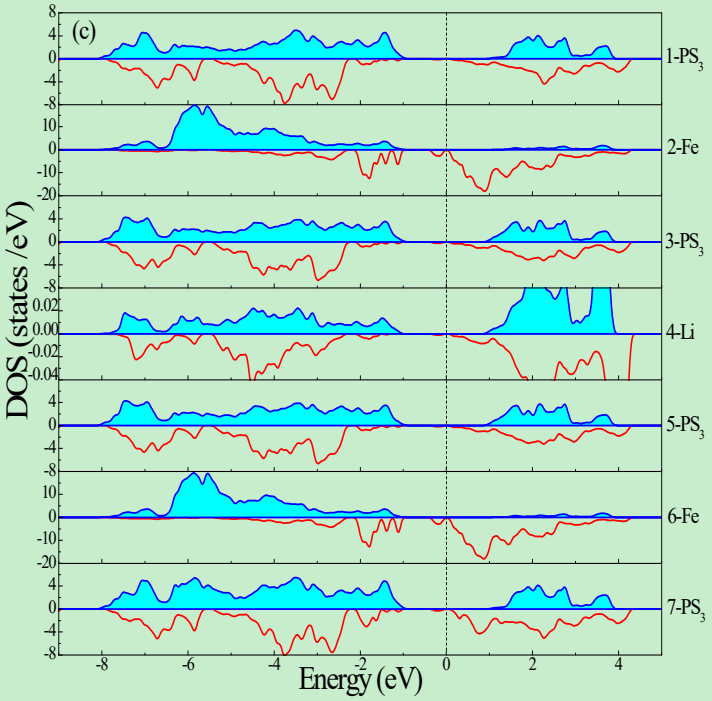

Fig. S7 Layer-resolved density of states of the 2D $FePS_3$ bilayer (a), the 1Li-intercalated $FePS_3$ bilayer (b), and the 2Li-intercalated $FePS_3$ bilayer.

Figs. S7(a), S7(b), and S7(c) show distinct characteristics of the layer-resolved DOSs (LDOSs) of the FPS, 1Li-, and 2Li-FPS bilayers, respectively. The VB DOS just below the E_F predominantly originates from the spin-up and spin-down states of strong hybridized Fe and S ions. The tops of VB of each layer are located at approximately -0.5 eV (-0.8 eV/-1.0 eV) for the 2D FPS bilayer (1Li-FPS bilayer/2Li-FPS bilayer), with no downward or upward shift can be seen. Importantly, the intercalated Li ions effectively broadened the VB DOS of Fe and PS_3 sublayers, indicating an enhanced hybridization between Fe and S/P ions. Fig. S7(a) demonstrates the non-conductivity of all Fe and PS_3 sublayers in the 2D FPS system. Compared to the PS_3 sublayer, the DOS of the Fe sublayer exhibits a greater level of asymmetry. For 1Li-FPS, the DOS at the Fermi level does not appear in the Li sublayer but is only found in the Fe sublayers and PS_3 sublayers, namely the electron generation is primarily concentrated in the upper and lower FPS monolayers. Itinerant electrons in the upper monolayer [see Fig. 2(a)] cannot penetrate the insulating Li sublayer into the lower monolayer, and vice versa. For 2Li-FPS, electrons can only be found in the two Fe sublayers, while the Li sublayer and PS_3 sublayers are all insulating at the E_F, *i.e.*, the two-dimensional electron is strictly confined within the Fe sublayers, and the Fe ions in the second and sixth sublayers exhibit perfect half-metallic characteristics.

References

1 D. Lançon, H. C. Walker, E. Ressouche, B. Quladdiaf, K. C. Rule, G. J. McIntyre, T. J. Hicks, H. M. Rønnow and A. R. Wildes, *Phys. Rev. B*, 2016, **94**, 214407.

2 C. R. S. Haines, M. J. Coak, A. R. Wildes, G. I. Lampronti, C. Liu, P. Nahai-Williamson, H. Hamidov, D. Daisenberger and S. S. Saxena, *Phys. Rev. Lett.*, 2018, **121**, 266801.

3 P. Sen and R. K. Chouhan, *Electron. Struct.*, 2020, **2**, 025003.

4 C. Murayama, M. Okabe, D. Urushihara, T. Asaka, K. Fukuda, M. Isobe, K. Yamamoto and Y. Matsushita, *J. Appl. Phys.*, 2016, **120**, 142114.

5 J. M. Zhang, Y. Z. Nie, X. G. Wang, Q. L. Xia and G. H. Guo, *J. Magn. Magn. Mater.*, 2021, **525**, 167687.

6 R. A. Evarestov and A. Kuzmin, *J. Comput. Chem.*, 2020, **41**, 1337-1344.

7 X. P. Wu, Z. Shen, W. Xiao, J. Q. Yang and C. S. Song, *J. Mater. Sci. Mater. El.*, 2022, **33**, 1871-1876.

8 E. Zanchini, *Inter. J. Thermal Sci.*, 2000, **39**, 110-116.

9 Q. Zhang, K. Hwangbo, C. Wang, Q. Jiang, J. H. Chu, H. Wen, D. Xiao and X. D. Xu, *Nano Lett.*, 2021, **21**, 6938-6945.

10 E. Geraffy, S. Zuri, M. M. Rybak, F. Horani, A. K. Budniak, Y. Amouyal, M. Birowska and E. Lifshitz, https://doi.org/10.21203/rs.3.rs-2014052/v1.

11 F. Kargar, E. A. Coleman, S. Ghosh, J. Lee, M. J. Gomez, Y. Liu, A. S. Magana, Z. Barani, A. Mohammadzadeh, B. Debnath, R. B. Wilson, R. K. Lake and A. A. Balandin, *ACS Nano*, 2020, **14**, 2424-2435.

12 Y. S. Zheng, X. X. Jiang, X. X. Xue, J. Y. Dai and Y. X. Feng, *Phys. Rev. B*, 2019, **100**, 174102.

13 S. Wang, B. B. Xiao, S. J. Shen, K. Song, Z. P. Lin, Z. P. Wang, Y. C. Chen and W. W. Zhong, *Nanoscale*, 2020, **12**, 14459-14464.

14 T. Das, S. Chakraborty and P. Sen, *Sustain. Energy Fuels*, 2022, **6**, 5321-5360.

15 T. Olsen, *J. Phys. D: App. Phys.*, 2021, **54**, 314001.

16 P. J. S. Foot, J. Suradi and P. A. Lee, *Mater. Res. Bull.*, 1980, **15**, 189-193.

17 R. Brec, D. M. Schleich, G. Ouvrard, A. Louisy and J. Rouxel, *Inorg. Chem.*, 1979, **18**, 1814-

1818.

18 S. Das, S. Chaturvedi, D. Tripathy, S. Grover, R. Singh, D. V. S. Muthu, S. Sampath, U. V. Waghmare and A. K. Sood, *J. Phys. Chem. Solids*, 2022, **164**, 110607.

19 Z. Yu, J. Peng, Y. H. Liu, W. X. Liu, H. F. Liu and Y. Q. Guo, *J. Mater. Chem. A*, 2019, **7**, 13928-13934.

20 Z. Z. Cheng, T. A. Shifa, F. M. Wang, Y. Gao, P. He, K. Zhang, C. Jiang, Q. L. Liu and J. He, *Adv. Mater.*, 2018, **30**, 1707433.

21 D. Mukherjee, P. M. Austeria and S. Sampath, *ACS Energy Lett.*, 2016, **1**, 367-372.

22 K. Z. Du, X. Z. Wang, Y. Liu, P. Hu, M. I. B. Utama, C. K. Gan, Q. H. Xiong and C. Kloc, *ACS Nano*, 2016, **10**, 1738-1743.

23 M. Q. Wang, J. Han, W. Liu, M. Kamiko and S. Yagi, *J. Alloys Compd.*, 2021, **883**, 160822.

24 V. Manríquez, P. Barahona, D. Ruiz and R. E. Avila, *Mater. Res. Bull.*, 2005, **40**, 475-483.

25 M. Barj, C. Sourisseau, G. Ouvrard and R. Brec, *Solid State Ionics*, 1983, **11**, 179-183.

26 H. L. Shen, Y. L. Cai, Z. T. Ma, P. Wang, B. K. Guo, J. P. Cheng, Q. Q. Li, H. T. Wang, Z. Y. Liu, A. M. Nie and J. S. Wu, *Carbon Energy*, 2023, **5**, e290.

27 N. C. Harms, K. A. Smith, A. V. Haglund, D. G. Mandrus, Z. X. Liu, H. S. Kim and J. L. Musfeldt, *ACS Appl. Electron. Mater.*, 2022, **4**, 3246-3255.

28 J. N. Tan, H. M. Hu, B. Cai, D. G. Xu and G. Ouyang, *Phys. Rev. B*, 2022, **106**, 195424.